PROTEIN ENGINEERING

Engineering extrinsic disorder to control protein activity in living cells

Onur Dagliyan,[1,2,3] Miroslaw Tarnawski,[4] Pei-Hsuan Chu,[3] David Shirvanyants,[2] Ilme Schlichting,[4] Nikolay V. Dokholyan,[1,2]* Klaus M. Hahn[3]*

Optogenetic and chemogenetic control of proteins has revealed otherwise inaccessible facets of signaling dynamics. Here, we use light- or ligand-sensitive domains to modulate the structural disorder of diverse proteins, thereby generating robust allosteric switches. Sensory domains were inserted into nonconserved, surface-exposed loops that were tight and identified computationally as allosterically coupled to active sites. Allosteric switches introduced into motility signaling proteins (kinases, guanosine triphosphatases, and guanine exchange factors) controlled conversion between conformations closely resembling natural active and inactive states, as well as modulated the morphodynamics of living cells. Our results illustrate a broadly applicable approach to design physiological protein switches.

Proteins have been engineered to respond to light or small molecules in living cells through a number of mechanisms, including oligomerization (*1*–*4*), control of targeting sequences (*1*, *5*, *6*), split proteins (*2*), sterically blocking the active site (*1*, *7*, *8*), and engineered allosteric control (*9*–*13*). Engineering allostery has the potential to be especially versatile and valuable, as sensory domains can be inserted where they do not interfere with normal protein interactions, more readily producing fully functional analogs to replace endogenous protein. Allosteric sites have been identified by using both screening approaches (*10*, *14*) and rational analysis of sequence conservation (*10*, *11*). A number of domains, including the light-sensitive LOV2 domain (*11*) and drug-responsive uniRapR domain (*12*, *13*) used here, have been applied. Nonetheless, it remains challenging to identify allosteric sites by rational analysis and to produce reversible, robust allosteric switches that have on and off states that replicate natural levels of protein activity. Here, we present a generalizable approach to identify surface loops where the disorder of the attached domain can be effectively transferred to the active site in a controlled fashion (harnessing extrinsic disorder) (*9*, *10*, *12*–*15*), to produce on and off states that mimic naturally occurring protein states.

In previous work, we identified an allosteric site in kinases where insertion of an engineered domain (uniRapR) conferred rapamycin-induced kinase activation (*12*, *13*). Insertion of the uniRapR domain rendered kinases catalytically inactive until the domain bound rapamycin (*12*, *13*, *16*). Molecular dynamics simulations indicated that the protein loop containing the insertion site was mechanically coupled to the adenosine triphosphate–binding site (*13*). We hypothesized that insertion of a light-responsive domain at the same site could lead to optogenetic control of kinases (Fig. 1A). We chose the LOV2 domain because the 10 Å spacing between its N and C termini enabled us to insert the domain with minimal perturbation into a loop (Fig. 1B) that connects parts of a tightly folded structural unit (two interacting antiparallel β-strands). The spacing between LOV2's termini becomes much more flexible upon irradiation, because of disordering of terminal helices (*17*, *18*); this could perturb the conformation of the loop and the β-strands. Introducing disorder into the loop would cause protein inhibition, rather than the activation caused by rapamycin-induced folding of the uniRapR domain (fig. S1). The light-induced conformational changes in LOV2 (3.8 kcal/mol of free energy) (*19*) should be more than sufficient to disorder portions of host proteins (fig. S2), whose overall stabilities are on the order of 5 to 15 kcal/mol (*20*).

We focused on Src kinase because of evidence that its activity is controlled by spatiotemporal dynamics in vivo (*16*, *21*). The LOV2 domain was inserted at Gly^{296} (G296) of a constitutively active Src mutant (Phe^{535} replaces Tyr^{535}; YF). We named the new Src analog PI-Src, for photo-inhibitable Src. In vitro kinase activity assays revealed that this LOV2-Src fusion was indeed strongly inhibited upon exposure to blue light (Fig. 1C). Light had no effect on the activity of kinase dead (KD) or constitutively active (YF) Src. Inhibition was not sensitive to small variations in linker length (fig. S3). To test PI-Src in living cells, we generated SYF cells (cells lacking the Src family members Src, Yes, and Fyn) expressing PI-Src(YF). Phosphotyrosine blots of cell lysates showed that irradiation inhibited phosphorylation of multiple Src substrates (Fig. 1C and fig. S4). Consistent with Src's reported roles in motility (*13*, *16*, *21*), irradiation reduced migration rates and caused reversible collapse of lamellipodia (fig. S5 and movie S1). Similar effects were produced by the Src inhibitor PP2 (fig. S5 and movie S2).

To investigate how distortion of the insertion loop led to a reduction in kinase activity, we built a structural model of PI-Src, and examined its light-induced conformational changes using discrete molecular dynamics (*22*, *23*). Although we expected to observe randomly distorted conformations of PI-Src in the lit state, we saw instead that the active and inactive states of PI-Src were strikingly similar to the crystal structures of active and inactive wild-type (WT) Src (correlation coefficient = 0.82) (Fig. 1D). This suggested that irradiation shifts PI-Src from its physiological active state to a conformation strongly resembling Src's native inactive state (fig. S6).

The physiologically relevant conformations of PI-Src raised the possibility of examining how Src controls the motility of living cells. We generated SYF cells expressing PI-Src(WT). In the dark, PI-Src(WT) showed the perinuclear distribution (Fig. 1E) typical of endogenous, inactive Src (*16*). Upon irradiation, the PI-Src translocated to focal adhesions at the cell periphery and induced changes in cell morphodynamics (increased protrusion and retraction, polarization, and polarized movement in some cases) (movie S3). Returning the cells to the dark reversed focal adhesion localization (Fig. 1E) but not effects on cell morphodynamics (fig. S7). It is thought that Src localization to focal adhesions is mediated by Src SH2-SH3 domains and is not dependent on kinase activity (*24*, *25*). The light-induced distortion of the catalytic domain that inhibits the kinase may also perturb autoinhibitory interactions, exposing the SH2 and SH3 domains; this likely generated the reversible focal adhesion localization we observed and suggested that focal adhesion localization was sufficient to affect cell morphodynamics even without catalytic activity. In support of this hypothesis, we found that PI-Src(KD) also translocated reversibly to adhesions and induced changes in morphodynamics upon irradiation and that elimination of the SH2 and SH3 domains from PI-Src (KD) prevented both focal adhesion localization and effects on cell morphodynamics (fig. S7). Movement away from focal adhesions, which occurred 30 to 40 s after irradiation was halted, indicated that the conformational change of PI-Src was reversible in cells (fig. S7) and was consistent with LOV2's rate of return to the dark conformation ($t_{1/2}$ = 18.5 s at 37°C in cells) (*26*). In contrast, effects on cell morphodynamics were retained for >20 min after irradiation was halted, potentially because of feedback kinetics and/or inactivation pathways not involving Src.

Controlling protein activity via LOV2 insertion would be much more valuable if it could be readily applied to multiple-protein families. We tested a more generalizable approach by identifying an allosteric site for LOV2 insertion in the Rho family guanosine triphosphatase (GTPase) Rac1. We focused on surface-exposed and evolutionarily nonconserved loops to avoid possible structural perturbations and asked whether these loops were mechanically coupled to the active site. For the

[1]Program in Molecular and Cellular Biophysics, University of North Carolina at Chapel Hill, Chapel Hill, NC 27599, USA. [2]Department of Biochemistry and Biophysics, University of North Carolina at Chapel Hill, Chapel Hill, NC 27599, USA. [3]Department of Pharmacology and Lineberger Comprehensive Cancer Center, University of North Carolina at Chapel Hill, Chapel Hill, NC 27599, USA. [4]Department of Biomolecular Mechanisms, Max Planck Institute for Medical Research, Jahnstrasse 29, 69120 Heidelberg, Germany.
*Corresponding author. Email: khahn@med.unc.edu (K.M.H.); dokh@email.unc.edu (N.V.D.)

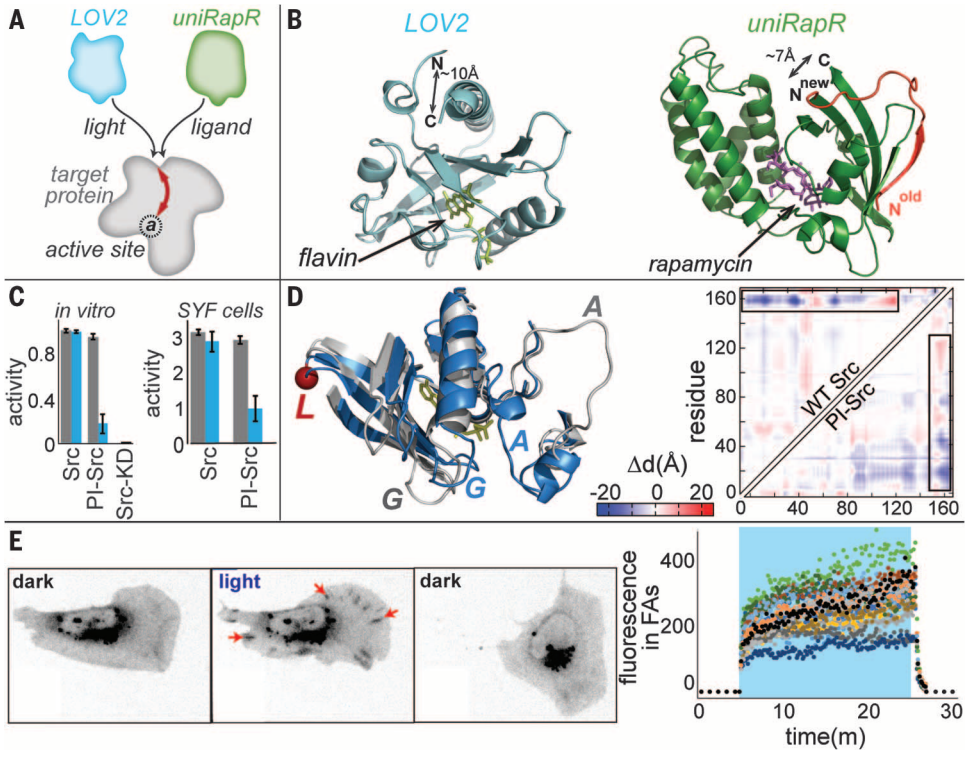

Fig. 1. Design concept and PI-Src. (**A**) Domains conferring either photoinhibition (LOV2), or activation induced by small molecules (uniRapR), function at the same allosteric site. (**B**) The termini of LOV2 and uniRapR domains are closely spaced for insertion. (**C**) Paxillin phosphorylation assays show that PI-Src's catalytic activity is inhibited upon irradiation. SYF cells expressing PI-Src(YF) show reduced phosphorylation of cell lysates blotted with antibody against phosphorylated Tyr (anti-pTyr). Blue denotes irradiation. Error bars show SEM (n = 3). (**D**) (Left) Inactive (blue) and active (gray) conformations of WT Src. The red circle (L) is the insertion site. Conformational changes were quantified by displaying the pairwise distance changes (Δd) between all residues as a heat map. (Right) The top left triangle shows distances for WT Src, computed from published crystal structures. The bottom triangle shows distances for PI-Src, determined using molecular dynamics simulations of the dark and lit states. Decreased distance (blue); increased distance (red). (**E**) In SYF cells, irradiation causes PI-Src(WT) to translocate to focal adhesions (FA, red arrows), edge movements to increase, and cells to polarize and translocate. When cells are returned to the dark, FA translocation is reversed but effects on morphodynamics persist. [Irradiation (blue); n = 18 cells; quantification in fig. S7.]

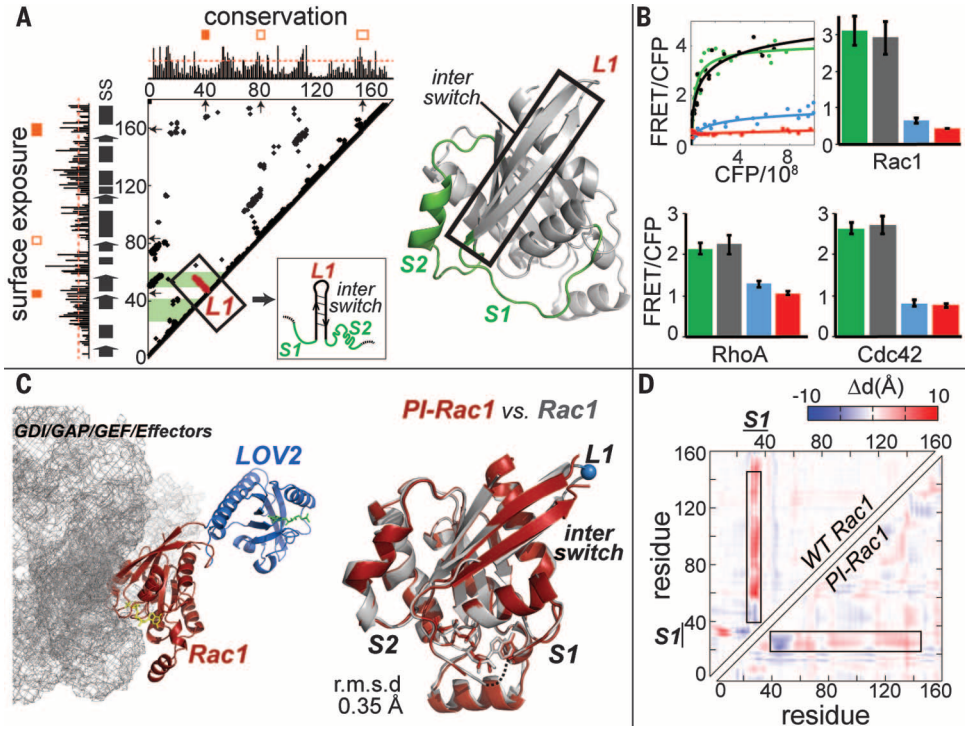

Fig. 2. Designing PI-GTPases. (**A**) Sequence conservation, surface exposure, loop "tightness," and contact maps were used to select insertion loops (fig. S9). Orange-filled boxes indicate loops fulfilling selection criteria [thresholds (red dashed lines); (box) S_1 and S_2, secondary structures]. In the scheme, lines extending perpendicular to the diagonal indicate loops (L) that connect tightly interacting elements of secondary structure. When these lines reached the active site (green bands) the loop was selected for testing. For PI-Rac1, we selected L1, which connects strands of the β-pleated sheet in the interswitch region. (**B**) GTPase activity in HEK293T cells reported using biosensors fused to PI-GTPases in a high-throughput assay. Dark-state mutant (gray); lit-state mutant (blue); T17N (Rac1 and Cdc42) and T19N (RhoA) dominant-negative mutants (red); wild-type GTPase-positive control (green). CFP x axis indicates expression level of biosensor-GTPase fusion. Error bars show SEM (n = 3). (**C**) (Left) Crystal structure of PI-Rac1 with interacting proteins (gray mesh); (right) structures of WT Rac1 (gray) and PI-Rac1 (red) are in excellent agreement. L1 loop is the LOV2 insertion loop. GDI, guanine nucleotide dissociation inhibitor; GAP, GTPase-activating protein. (**D**) Map showing interresidue distances for WT Rac1 versus PI-Rac1, which suggest that these molecules undergo similar conformational changes.

kinase analogs above, we found that both dynamic coupling analysis (*12*) and a static contact map analysis (figs. S8 and S9) were effective in identifying mechanically coupled loops. (The latter offers a simpler approach accessible to many laboratories.) Dynamic coupling and static contact map analyses indicated several loops in Rac1 (Fig. 2A and fig. S10); however, much of the surface of Rac1 is used to interact with other proteins, which limits the loops appropriate for insertion. Considering all these criteria, we selected loop L1, which connects β-strands between

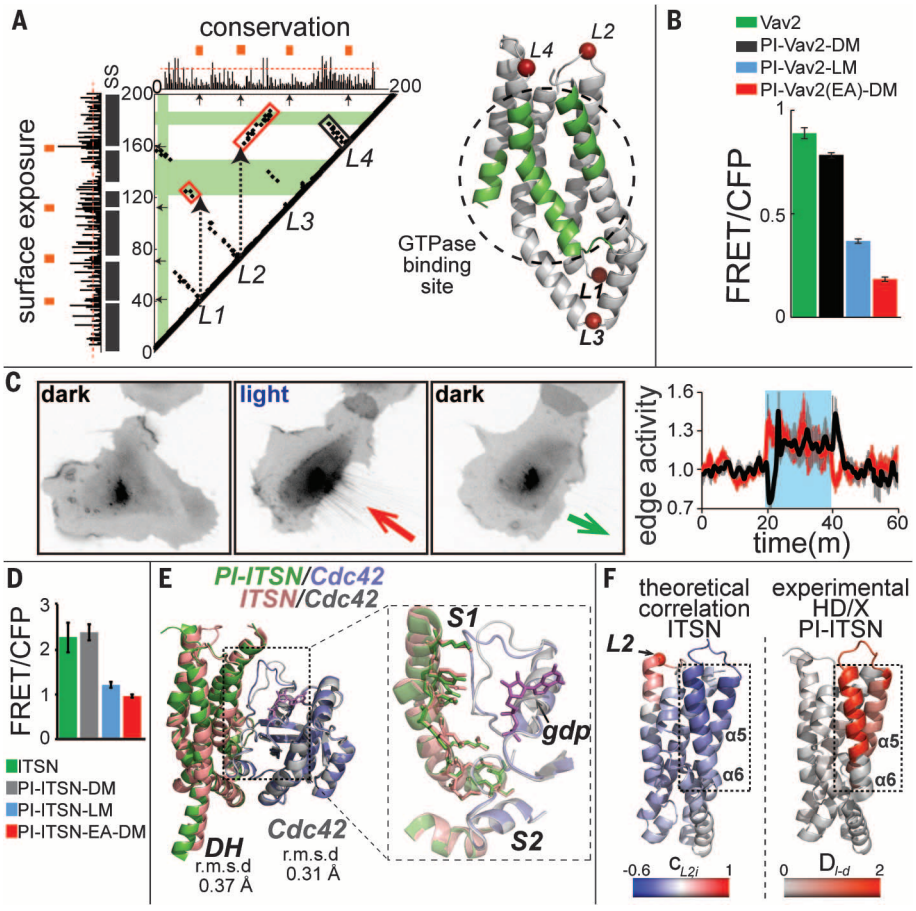

Fig. 3. Designing PI-GEFs. (**A**) Computational analysis of the Vav2 catalytic DH domain. (Left) Black and red boxes indicate local and nonlocal interactions (fig. S9) that mediate coupling between loops and the active site. (Right) Structural model of the Vav2 DH domain showing insertion loops and the active site (green). (**B**) In living cells, PI-Vav2 was inhibited in the lit state. DM and LM, dark and lit mutants; EA, E200A/K333A dominant-negative mutant. Error bars show SEM (n = 3). (**C**) (Left) Reversible retraction induced by irradiation of PI-Vav2 in HeLa cells (n = 9); retraction (red arrow), protrusion (black arrow). (**D**) High-content live-cell imaging showed that PI-ITSN was inhibited in the lit state. EA, E1244A catalytically inactive mutant. Error bars show SEM (n = 3). (**E**) (Left) Crystal structure of PI-ITSN (L2) in complex with Cdc42 superimposed on the WT ITSN:Cdc42 complex. (Inset, right) Purple, gdp, guanosine diphosphate. (**F**) Comparison of deuterium exchange (HD/X) results and dynamic coupling computed using molecular dynamics simulations. $C_{L2,I}$ corresponds to the correlation coefficient between the motion of the L2 loop and the motions of each residue. $D_{I\text{-}d}$ corresponds to the differences in relative deuteration levels in the dark and light.

the S1 and S2 regions (Fig. 2A). L1 was similar to the insertion loop of Src in that it connected interacting secondary structures, enabling efficient propagation of structural changes from the inserted domain to the host protein. All the examples that follow indicate that such "tight loops" are useful insertion sites (figs. S9 and S11).

To test the efficacy of LOV2 insertion into the L1 loop, we incorporated the Rac1 analog into a previously characterized fluorescence resonance energy transfer (FRET) biosensor of Rac1 activity (*27*) (donor fluorescent protein fused to PI-Rac1 and FRET acceptor fused to a fragment from p21-activated kinase that specifically binds activated Rac1). PI-Rac1 containing a dark-state LOV2 mutation was activated by the upstream guanine exchange factor (GEF) Vav2, whereas activation of a lit-state mutant was substantially reduced (Fig. 2B). Even when an activating mutation (Q61L) was introduced in Rac1, the lit-state LOV2 mutant showed strong inhibition (fig. S12). For physiologically relevant studies, we used PI-Rac1 to replace endogenous Rac1 in Rac1-depleted fibroblasts. Irradiation produced reversible cell edge retraction, initially as indentations closely spaced along the edge, and then broad retraction of entire lamellae (fig. S12 and movies S4 and S5). We also generated switches from the Rho family GTPases RhoA and Cdc42, using insertion in the same loop. Both showed effective light-induced inhibition in live cells (Fig. 2B, fig. S13, and movies S6 and S7).

To probe the mechanism of photoinhibition, we determined the crystal structure of dark-state PI-Rac1 and examined lit and dark conformational changes using molecular dynamics. The crystal structure showed that LOV2 was placed where it did not interfere with Rac1 binding to regulatory or effector proteins (Fig. 2C, fig. S14, and table S1). Notably, the dark state–activated structure was almost identical to that of activated WT Rac1, with a root mean square deviation (RMSD) of only 0.35 Å (Fig. 2C). Molecular dynamics showed that the conformational change between dark and irradiated PI-Rac1 manifested mainly in the S1 and S2 switch regions and that the conformational changes of PI-Rac1 and WT Rac1 were remarkably similar (Fig. 2D and fig. S15). Together, these studies suggested that opto-allosteric perturbation of Rac1, like Src, caused switching between naturally occurring active and inactive states.

We next targeted another protein family, GEFs, beginning with the Rac1 activator Vav2. GEFs present a different challenge in that they induce a conformational change through GTPase binding to a broad area involving many relatively weak interactions. Computational analysis of Vav2's GTPase-binding DH domain revealed three potential insertion loops (Fig. 3A and fig. S16). We used loop L4 for LOV2 insertion because it produced the most effective switch. PI-Vav2 was tested in living cells by examining its effects on a Rac1 biosensor (Fig. 3B). The activities of the PI-Vav2 dark- and lit-state mutants resembled those of different activated and inactivated Vav2 mutants (Fig. 3B and figs. S17 and S18). Pull-down assays confirmed that PI-Vav2 was inhibited upon irradiation (fig. S17) and that irradiation of PI-Vav2 in HeLa cells produced rapid and reversible retraction (Fig. 3C and movie S8). Insertion of LOV2 into L1 or L2 also produced effective PI-Vav2 constructs, but insertion of LOV2 into a loop that was not "tight" produced no switch (fig. S18). The same analysis was used to create two other photoinhibitable GEFs: GEF-H1, a Rho GEF, and Intersectin1(ITSN), a Cdc42 GEF (Fig. 3D and figs. S19 to S21).

Unlike kinase and GTPase catalytic domains, the GEF catalytic domains do not undergo major intradomain conformational changes. Instead, they are regulated sterically by autoinhibitory domains. To investigate the light-mediated structural changes of PI-ITSN (L2), we determined the crystal structures of PI-ITSN alone and in complex with Cdc42 (Fig. 3E, fig. S22, and table S2). PI-ITSN and WT ITSN were structurally similar, with a backbone RMSD of 0.37 Å. The structure of Cdc42 in the ITSN:Cdc42 complex and in the PI-ITSN:Cdc42 complex were similar, with an RMSD of only 0.31 Å. The interface between ITSN and Cdc42 was also in excellent agreement in the two structures, with an RMSD of 0.36 Å (Fig. 3E). The crystal structure of the PI-ITSN:Cdc42 complex was consistent with the shapes of the PI-ITSN:Cdc42 complex and PI-ITSN in solution, constructed ab initio by small angle x-ray scattering (fig. S23).

Molecular dynamics simulations of ITSN and PI-ITSN revealed that the motions of helices α5 and α6, part of the active site, correlate with the motions of the insertion loop (Fig. 3F), and hydrogen or deuterium exchange coupled to mass spectrometry showed light-induced destabilization of these helices (Fig. 3F and figs. S24 to S26). These results suggest that native ITSN and Cdc42 interactions are maintained in PI-ITSN

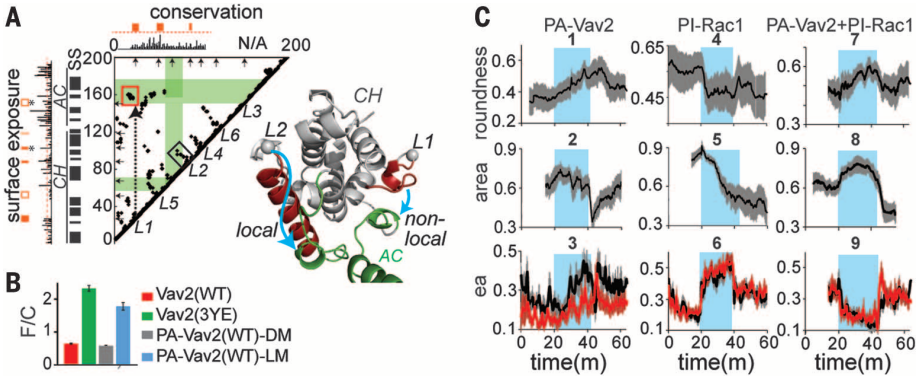

Fig. 4. Designing PA-Vav2 and multiplexed control in living cells. (**A**) (Left) Computational analysis of Vav2's AID indicated that loops L1 and L2 are coupled to the active site (green) through nonlocal (red box) and local (black box) interactions. CH and AC denote calponin-homology and acidic motifs. (Right) A structural model of the AID showing the connection of L1 and L2 to the active site. (**B**) PA-Vav2 is activated in the lit state, assayed as in Fig. 2B. Error bars show SEM ($n = 3$). (**C**) Effects of irradiation and cessation of irradiation on cells expressing PA-Vav2 alone, PI-Rac1 alone, or both in the same cell. Blue box denotes irradiation, ea denotes edge activity, and envelopes show SEM ($n = 15$ for PA-Vav2; $n = 18$ for PI-Rac1; $n = 17$ for PA-Vav2+PI-Rac1).

and support an allosteric connection between the insertion loop and important active-site residues.

We also inserted the uniRapR domain in GEFs, to activate GEFs with rapamycin. Vav2, ITSN, Asef, p115, and Tiam1 all showed rapamycin-induced GTPase binding in pull-down assays (fig. S27). Titrating uniRapR-Vav2 with saturating rapamycin in human embryonic kidney–293T (HEK293T) cells produced dose-dependent activation of a Rac1 biosensor (fig. S27), and fibroblasts stably expressing uniRapR-Vav2 or uniRapR-ITSN-produced protrusions and ruffles upon rapamycin addition (fig. S27 and movie S9).

Successful photoinhibition suggested that we might also use allosteric control to activate proteins with light. GEFs, and many other proteins, are regulated by intramolecular interactions of autoinhibitory domains (AIDs), which might be turned on and off allosterically. Analyzing the CH portion of Vav2's AID showed two potential insertion loops (Fig. 4A and fig. S28). We inserted LOV2 in these and in three additional loops not predicted to control activity (fig. S29). In live-cell assays using Rac1 biosensor activity as a readout, only the computed insertion sites produced robust switches (Fig. 4B and fig. S29). In fibroblasts, Vav2 photoactivation induced rounding and lamellae formation rather than the retractions produced by photoinhibition. Upon removal of light, PA-Vav2 cells underwent marked contractions (panels 1 and 2 in Fig. 4C, fig. S30, and movie S10). These results demonstrated that a protein can be allosterically activated by light through control of its AID.

With optogenetics, effects of protein manipulation can be assayed rapidly, before the cell has a chance to compensate as it does with genetic manipulations. We tested whether photoactivation and photoinhibition could be combined, to assay how photoactivation of one protein is affected by downstream inhibition of another. Unlike the rounding and large lamellae produced by irradiating PA-Vav2 (panel 1 in Fig. 4C and movie S10), irradiating PI-Rac1 cells (produced via knockdown and rescue of Rac1) caused retraction (panels 4 and 5 in Fig. 4C and movie S5), with formation of a complex perimeter and increased velocity of both retractions and protrusions (panel 6 in Fig. 4C). When PA-Vav2 and PI-Rac1 were irradiated in the same cell, area and roundness responded similarly to PA-Vav2 alone, but the cell edge showed a phenotype clearly different from that produced by the individual proteins, with a strong reduction in edge dynamics during irradiation (panels 7 to 9 in Fig. 4C, movie S11, and fig. S30). Thus, PI-Rac1 was being activated and affecting results of Vav2 activation. Interpretation will require further study, but these results are consistent with recent work showing that Vav2 can act independent of Rac1 (*28*–*30*).

In summary, we have controlled proteins with light or small molecules in living cells by harnessing order/disorder transitions. Sensory domains were inserted into tight, nonconserved, surface loops that are allosterically coupled to active sites. Engineered proteins switched between naturally occurring, physiologically relevant active and inactive states, generating effective tools to manipulate living cells.

REFERENCES AND NOTES

1. M. Weitzman, K. M. Hahn, *Curr. Opin. Cell Biol.* **30**, 112–120 (2014).
2. L. A. Banaszynski, T. J. Wandless, *Chem. Biol.* **13**, 11–21 (2006).
3. A. Levskaya, O. D. Weiner, W. A. Lim, C. A. Voigt, *Nature* **461**, 997–1001 (2009).
4. M. J. Kennedy *et al.*, *Nat. Methods* **7**, 973–975 (2010).
5. H. Yumerefendi *et al.*, *Nat. Chem. Biol.* **12**, 399–401 (2016).
6. D. Niopek *et al.*, *Nat. Commun.* **5**, 4404 (2014).
7. Y. I. Wu *et al.*, *Nature* **461**, 104–108 (2009).
8. X. X. Zhou, H. K. Chung, A. J. Lam, M. Z. Lin, *Science* **338**, 810–814 (2012).
9. J. H. Choi, A. H. Laurent, V. J. Hilser, M. Ostermeier, *Nat. Commun.* **6**, 6968 (2015).
10. M. Ostermeier, *Curr. Opin. Struct. Biol.* **19**, 442–448 (2009).
11. J. Lee *et al.*, *Science* **322**, 438–442 (2008).
12. A. V. Karginov, F. Ding, P. Kota, N. V. Dokholyan, K. M. Hahn, *Nat. Biotechnol.* **28**, 743–747 (2010).
13. O. Dagliyan *et al.*, *Proc. Natl. Acad. Sci. U.S.A.* **110**, 6800–6804 (2013).
14. B. L. Oakes *et al.*, *Nat. Biotechnol.* **34**, 646–651 (2016).
15. C. L. Tucker, S. Fields, *Nat. Biotechnol.* **19**, 1042–1046 (2001).
16. P. H. Chu *et al.*, *Proc. Natl. Acad. Sci. U.S.A.* **111**, 12420–12425 (2014).
17. S. M. Harper, L. C. Neil, K. H. Gardner, *Science* **301**, 1541–1544 (2003).
18. A. S. Halavaty, K. Moffat, *Biochemistry* **46**, 14001–14009 (2007).
19. X. Yao, M. K. Rosen, K. H. Gardner, *Nat. Chem. Biol.* **4**, 491–497 (2008).
20. A. R. Fersht, L. Serrano, *Curr. Opin. Struct. Biol.* **3**, 75–83 (1993).
21. M. P. Playford, M. D. Schaller, *Oncogene* **23**, 7928–7946 (2004).
22. Y. Zhou, M. Karplus, *Nature* **401**, 400–403 (1999).
23. F. Ding, D. Tsao, H. Nie, N. V. Dokholyan, *Structure* **16**, 1010–1018 (2008).
24. V. J. Fincham, M. C. Frame, *EMBO J.* **17**, 81–92 (1998).
25. V. G. Brunton *et al.*, *Cancer Res.* **65**, 1335–1342 (2005).
26. H. Wang *et al.*, *Nat. Methods* **13**, 755–758 (2016).
27. M. Machacek *et al.*, *Nature* **461**, 99–103 (2009).
28. G. L. Razidlo, B. Schroeder, J. Chen, D. D. Billadeau, M. A. McNiven, *Curr. Biol.* **24**, 86–93 (2014).
29. K. Abe *et al.*, *J. Biol. Chem.* **275**, 10141–10149 (2000).
30. T. Samson, C. Welch, E. Monaghan-Benson, K. M. Hahn, K. Burridge, *Mol. Biol. Cell* **21**, 1629–1642 (2010).

ACKNOWLEDGMENTS

This work was supported by NIH grants P01-GM103723 and P41-EB002025 (K.M.H.), R01GM080742 (N.V.D.), and by Deutsche Forschungsgemeinschaft grant FOR1279 (I.S.). O.D. is a Howard Hughes Medical Institute International Student Research Fellow. X-ray data were collected at the Swiss Light Source, beamline X10SA and X12SA, Paul Scherrer Institute, Villigen, Switzerland. We thank A. Menzel and T. Barends for collecting the small angle x-ray scattering data, and M. Shobair for his help with PI-Vav2 simulations. Atomic coordinates and structure factors have been deposited in the Protein Data Bank under accession codes: 5HZJ (PI-ITSN1–WT), 5HZI (PI-ITSN1–C450M), 5HZK (PI-ITSN1–WT: Cdc42), and 5HZH (PI-Rac1–C450A). O.D., N.V.D., and K.M.H. designed the research; M.T. performed the crystallographic work and conducted hydrogen-deuterium exchange coupled to mass spectrometry assays under the directions of I.S. who collected the x-ray data; P.-H.C. helped the characterization of PI-Src; D.S. conducted the simulations of PI-Src; O.D. performed all experiments and computations not listed above; O.D. and K.M.H. wrote the manuscript with input from all authors. The constructs described in this paper are available from K.M.H under a material transfer agreement with the University of North Carolina–Chapel Hill.

SUPPLEMENTARY MATERIALS

www.sciencemag.org/content/354/6318/1441/suppl/DC1
Materials and Methods
Tables S1 to S3
Figs. S1 to S30
References (*31*–*63*)
Movies S1 to S11

12 June 2016; accepted 16 November 2016
10.1126/science.aah3404

Editor's Summary

Engineering control of cellular proteins

The ability to switch proteins between active and inactive conformations can give insight into their function. Dagliyan *et al.* present a method to insert domains that control protein activity. They computationally identified protein loops that are coupled to the active site. Sensory domains inserted into these loops could modulate protein activity when their conformation was changed by light or ligand binding. The authors engineered domains into three different classes of proteins involved in cell signaling and found that switching the proteins between active and inactive states could control the shape and movement of living cells.

Science, this issue p. 1441